Electronic Supplementary Information

for

N-C Bond Formation Between Two Anilines Coordinated to a Ruthenium Center in a *Cis*-form Affording a 3,5-Cyclohexadiene-1,2-diimine Moiety

*Nozomi Tomioka, Shinkoh Nanbu, Tomoyo Misawa-Suzuki and Hirotaka Nagao**

Department of Materials and Life Sciences, Faculty of Science and Technology,

Sophia University

7-1 Kioi-cho, Chiyoda-ku, Tokyo 102-8554 (Japan)

NMR spectroscopy

Dianiline complexes and diimine complexes (10 mg) were dissolved in 1 cm^3 of DMSO-d^6 (a and b), methanol-d^4 (c) and nitromethane-d^3 (d and e), respectively. The solutions were transferred to a cell (ϕ = 5 mm) with simple filtration using a syringe equipped with a membrane filter. ^{1}H and ^{13}C NMR spectra were shown in Fig. S1 and S2.

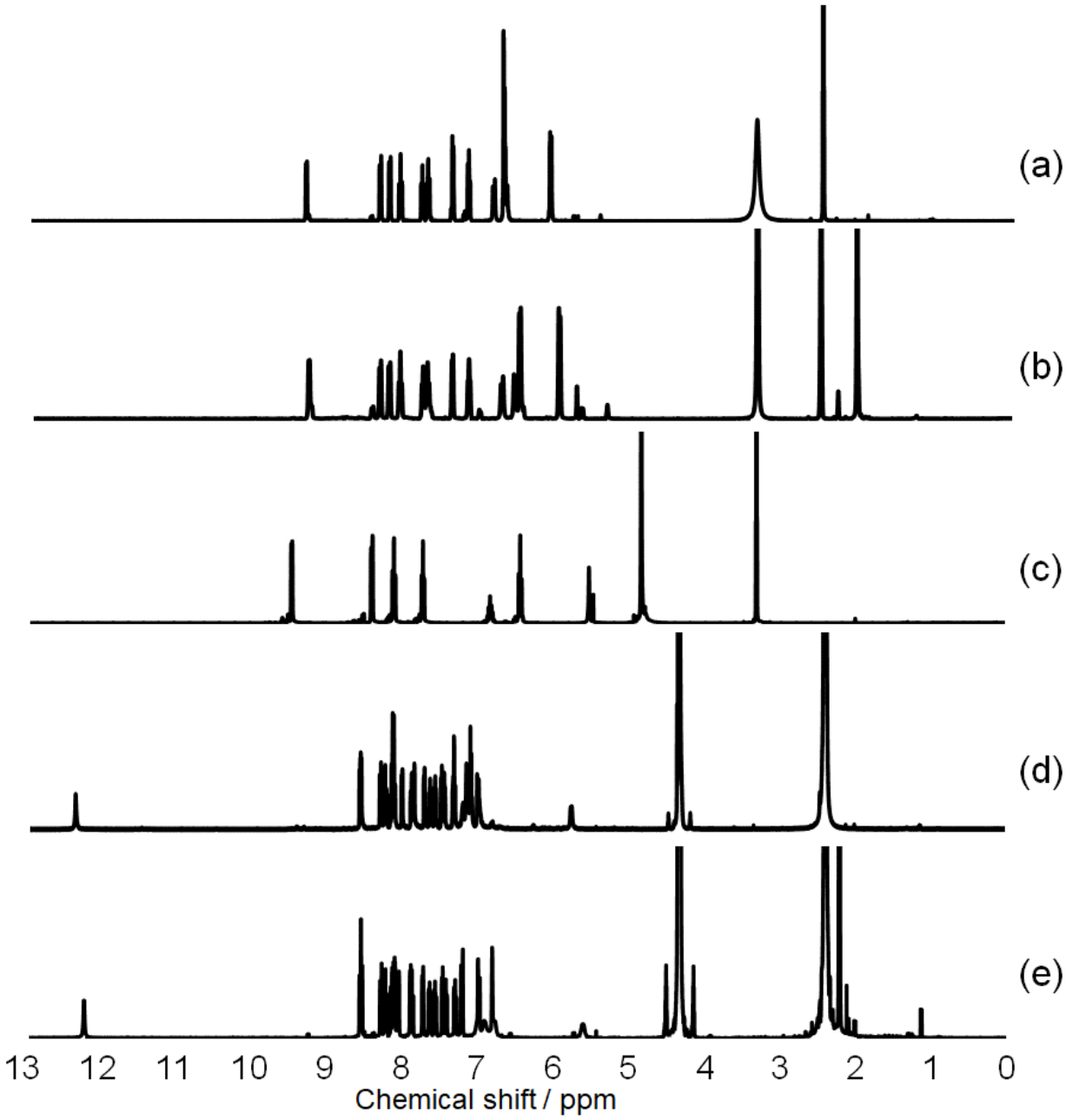

Fig. S1 ^{1}H NMR spectra.

(a) *cis*-[$Ru^{II}(NH_2C_6H_5)_2(bpy)_2$]($CF_3SO_3$)$_2$ [**1**](CF_3SO_3)$_2$, (b) *cis*-[$Ru(NH_2C_6H_4(4\text{-}CH_3))_2(bpy)_2$]-($CF_3SO_3$)$_2$ [**2**](CF_3SO_3)$_2$, (c) *trans*-[$Ru(NH_2C_6H_3(2,6\text{-}F_2))_2(bpy)_2$]($CF_3SO_3$)$_2$ [**3**](CF_3SO_3)$_2$, (d) *cis*-[Ru^{II}($N$$HC_6H_4$$N$$C_6H_5$)$(bpy)_2$]($PF_6$)$_2$ [**4**](PF_6)$_2$ and (e) *cis*-[Ru^{II}($N$$HC_6H_3(4\text{-}CH_3)$$N$$C_6H_4(4\text{-}CH_3)$)-$(bpy)_2$]($PF_6$)$_2$ [**5**](PF_6)$_2$.

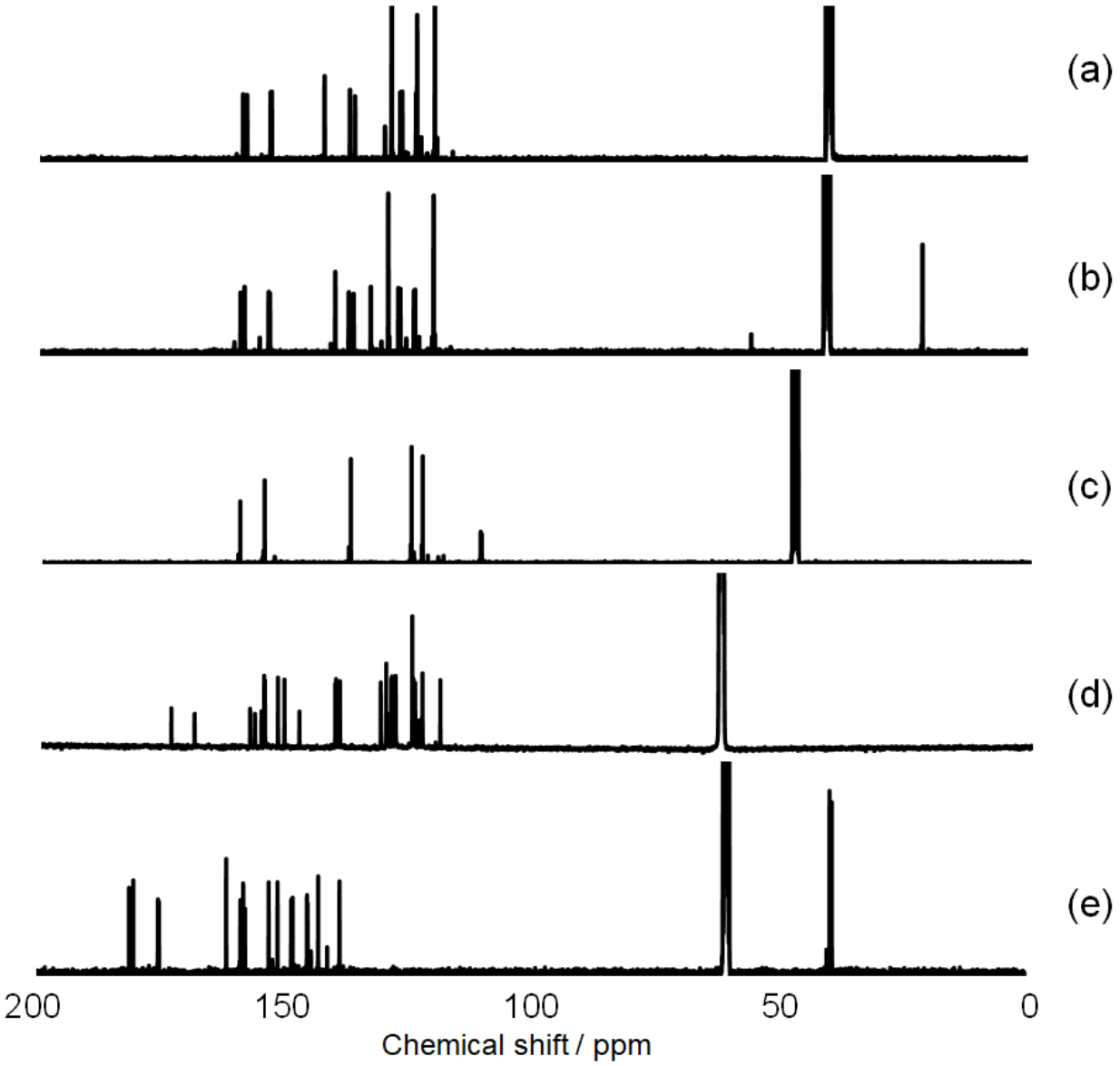

Fig. S2 ^{13}C NMR spectra.

(a) *cis*-[$Ru^{II}(NH_2C_6H_5)_2(bpy)_2$]($CF_3SO_3$)$_2$ [**1**](CF_3SO_3)$_2$, (b) *cis*-[$Ru(NH_2C_6H_4(4\text{-}CH_3))_2(bpy)_2$]-($CF_3SO_3$)$_2$ [**2**](CF_3SO_3)$_2$, (c) *trans*-[$Ru(NH_2C_6H_3(2,6\text{-}F_2))_2(bpy)_2$]($CF_3SO_3$)$_2$ [**3**](CF_3SO_3)$_2$, (d) *cis*-[Ru^{II}(*N*HC_6H_4*N*C_6H_5)$(bpy)_2$](PF_6)$_2$ [**4**](PF_6)$_2$ and (e) *cis*-[Ru^{II}(*N*$HC_6H_3(4\text{-}CH_3)$*N*$C_6H_4(4\text{-}CH_3)$)-$(bpy)_2$](PF_6)$_2$ [**5**](PF_6)$_2$.

IR spectroscopy

IR spectra for dianiline and diimine complexes were obtained by integration of sixteen times in the range from 4000 to 400 cm^{-1}.

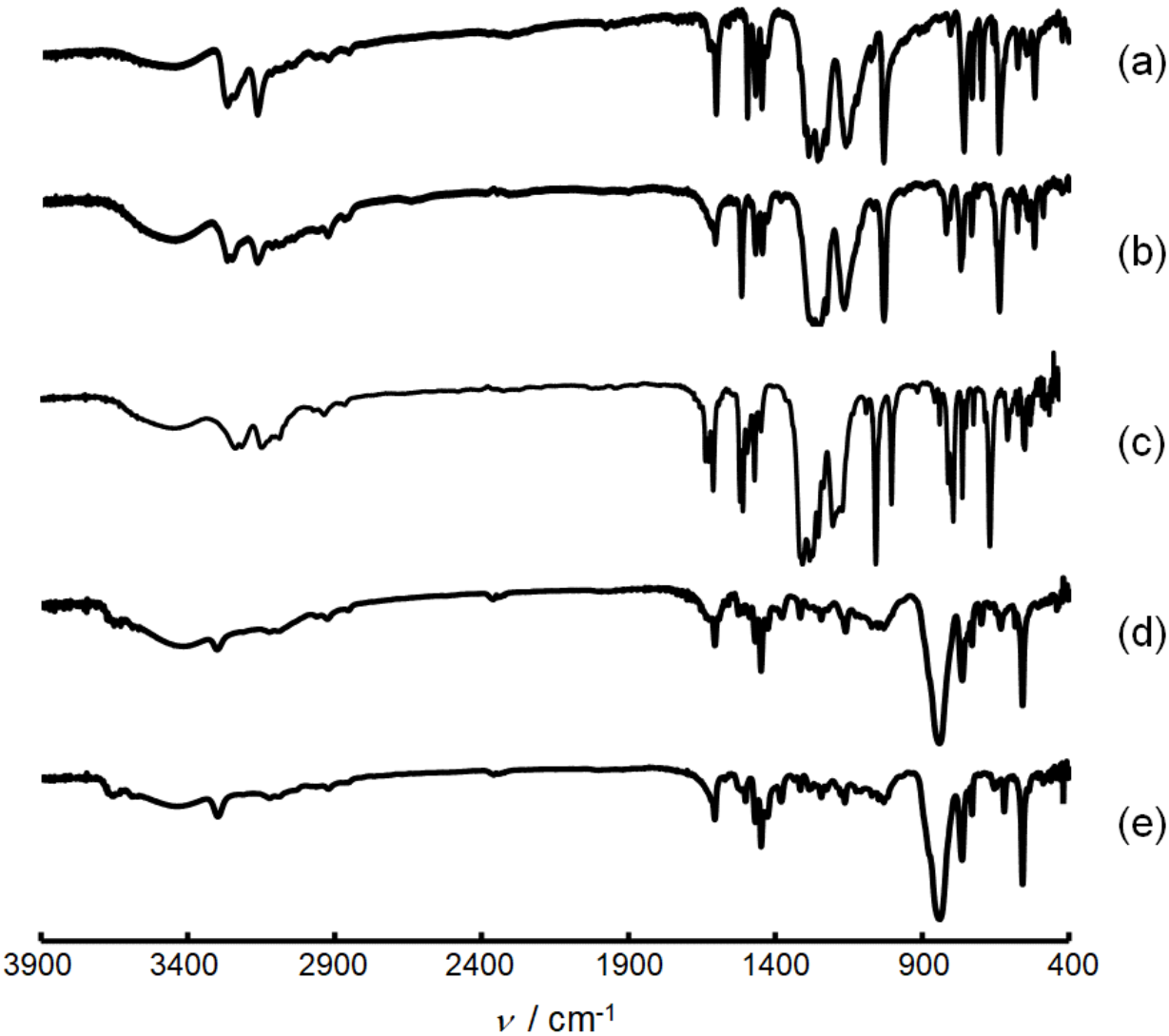

Fig. S3 IR spectra of *cis*-$[Ru^{II}(NH_2C_6H_5)_2(bpy)_2](CF_3SO_3)_2$ [**1**]$(CF_3SO_3)_2$ (a), *cis*-$[Ru(NH_2C_6H_4(4\text{-}CH_3))_2(bpy)_2](CF_3SO_3)_2$ [**2**]$(CF_3SO_3)_2$ (b), *trans*-$[Ru(NH_2C_6H_3(2,6\text{-}F_2))_2(bpy)_2](CF_3SO_3)_2$ [**3**]$(CF_3SO_3)_2$ (c), *cis*-$[Ru^{II}(NHC_6H_4NC_6H_5)(bpy)_2](PF_6)_2$ [**4**]$(PF_6)_2$ (d) and *cis*-$[Ru^{II}(NHC_6H_3(4\text{-}CH_3)NC_6H_4(4\text{-}CH_3))(bpy)_2](PF_6)_2$ [**5**]$(PF_6)_2$ (e).

UV-vis spectroscopy

UV-vis spectra were obtained using a square quartz cell with an optical path length of 1.0 cm. Electronic spectra of four dianiline and diimine complexes in H_2O are shown in Fig. S4 and Table S1. UV-vis spectra of $[Ru^{II}(NH_2C_6H_5)_2(bpy)_2]^{2+}$ [**1**]$^{2+}$ and $[Ru^{II}(NHC_6H_4NC_6H_5)(bpy)_2]^{2+}$ [**4**]$^{2+}$ were calculated by time-dependent density-functional theory (Fig. S5 and S6).

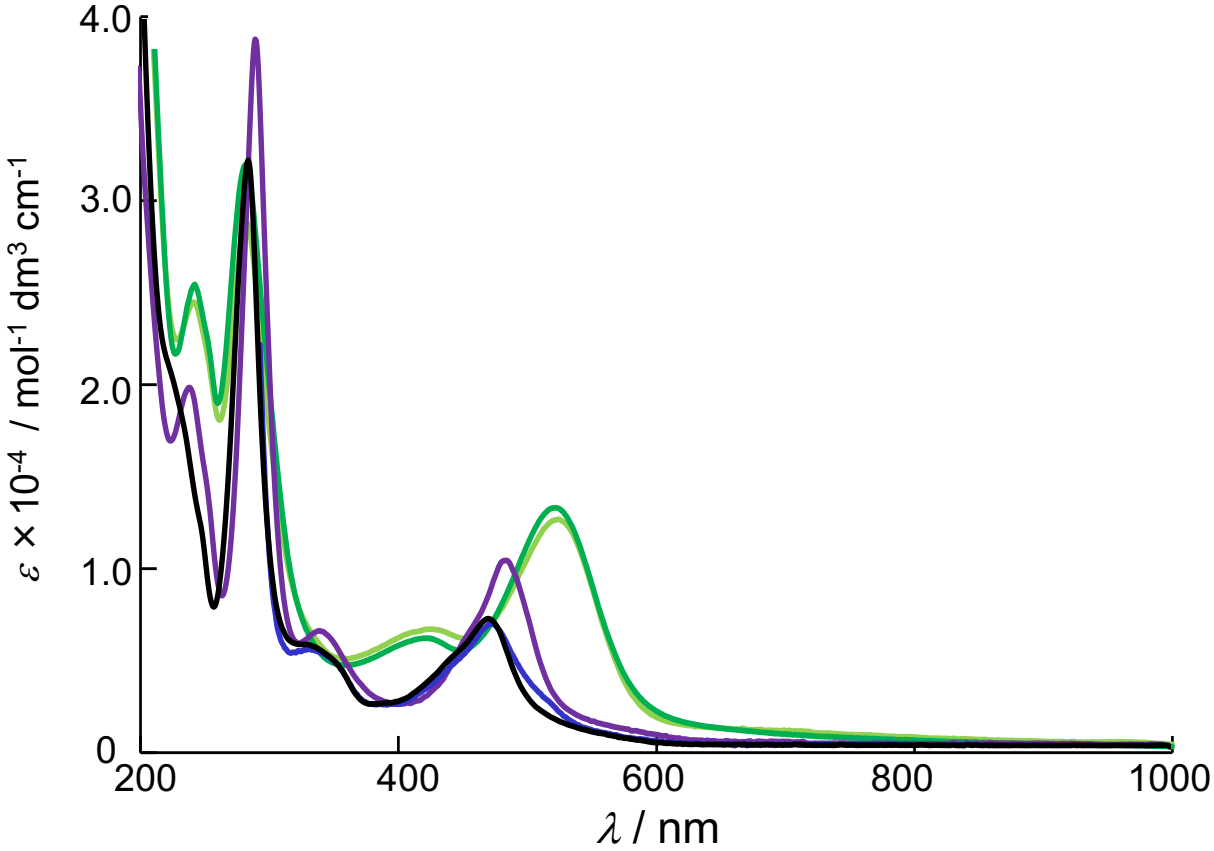

Fig. S4 UV-vis spectra of *cis*-$[Ru^{II}(NH_2C_6H_5)_2(bpy)_2](CF_3SO_3)_2$ [**1**]$(CF_3SO_3)_2$ (black), *cis*-$[Ru(NH_2C_6H_4(4\text{-}CH_3))_2(bpy)_2](CF_3SO_3)_2$ [**2**]$(CF_3SO_3)_2$ (blue), *trans*-$[Ru(NH_2C_6H_3(2,6\text{-}F_2))_2\text{-}(bpy)_2](CF_3SO_3)_2$ [**3**]$(CF_3SO_3)_2$ (purple), *cis*-$[Ru^{II}(NHC_6H_4NC_6H_5)(bpy)_2](PF_6)_2$ [**4**]$(PF_6)_2$ (green) and *cis*-$[Ru^{II}(NHC_6H_3(4\text{-}CH_3)NC_6H_4(4\text{-}CH_3))(bpy)_2](PF_6)_2$ [**5**]$(PF_6)_2$ (light green).

Table S1 Maximal absorption wavelengths of ruthenium complexes

complex	λ_{max} ($\varepsilon \times 10^{-4}$ / mol^{-1} dm^3 cm^{-1})	
cis-$[Ru^{II}(NH_2C_6H_5)_2(bpy)_2](CF_3SO_3)_2$ [**1**]$(CF_3SO_3)_2$	340 (0.537)	479 (0.673)
cis-$[Ru(NH_2C_6H_4(4\text{-}CH_3))_2(bpy)_2](CF_3SO_3)_2$ [**2**]$(CF_3SO_3)_2$	340 (0.532)	481 (0.669)
trans-$[Ru(NH_2C_6H_3(2,6\text{-}F_2))_2(bpy)_2](CF_3SO_3)_2$ [**3**]$(CF_3SO_3)_2$	341 (0.616)	487 (1.02)
cis-$[Ru^{II}(NHC_6H_4NC_6H_5)(bpy)_2](PF_6)_2$ [**4**]$(PF_6)_2$	421 (0.622)	520 (1.33)
cis-$[Ru(NHC_6H_3(4\text{-}CH_3)NC_6H_4(4\text{-}CH_3))(bpy)_2](PF_6)_2$ [**5**]$(PF_6)_2$	425 (0.672)	524 (1.27)

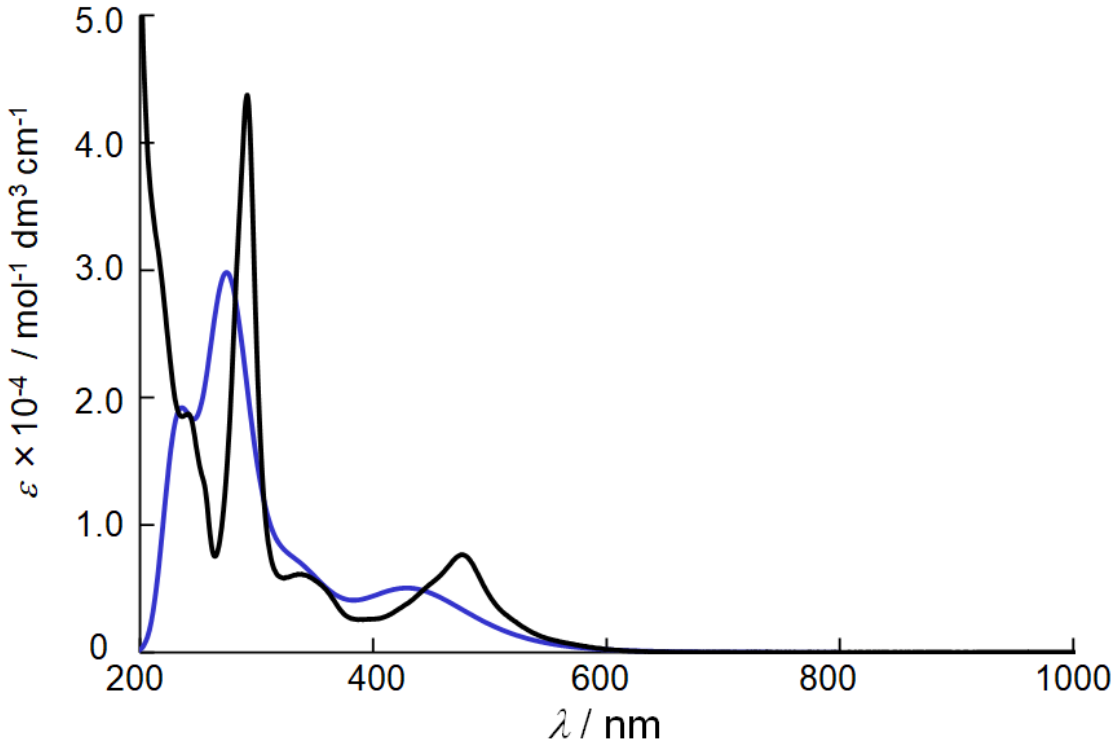

Fig. S5 UV-vis spectra of *cis*-$[Ru^{II}(NH_2C_6H_5)_2(bpy)_2]^{2+}$ $[\mathbf{1}]^{2+}$ (found value: black, calculated value: blue).

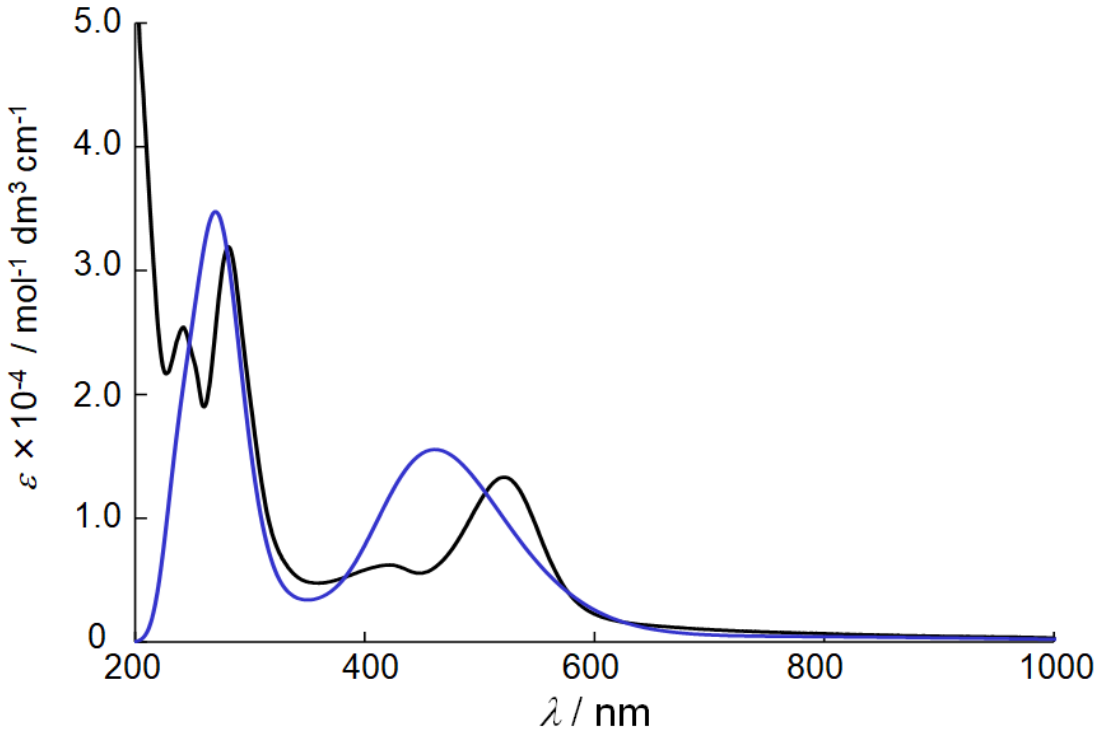

Fig. S6 UV-vis spectra of *cis*-$[Ru^{II}(NHC_6H_4NC_6H_5)(bpy)_2]^{2+}$ $[\mathbf{4}]^{2+}$ (found value: black, calculated value: blue).

Electrochemical measurements

Cyclic voltammograms of *cis*-[$Ru^{II}(NH_2C_6H_5)_2(bpy)_2$]($CF_3SO_3$)$_2$ [**1**](CF_3SO_3)$_2$ in water-dimethyl sulfoxide (2:3 (*v*:*v*)) mixed solutions at pH 2.77, 4.65, 6.06 and 7.90 were shown in Fig. S7. Pourbaix diagram is plotted on pH vs. the oxidation potentials as shown in Fig. S8.

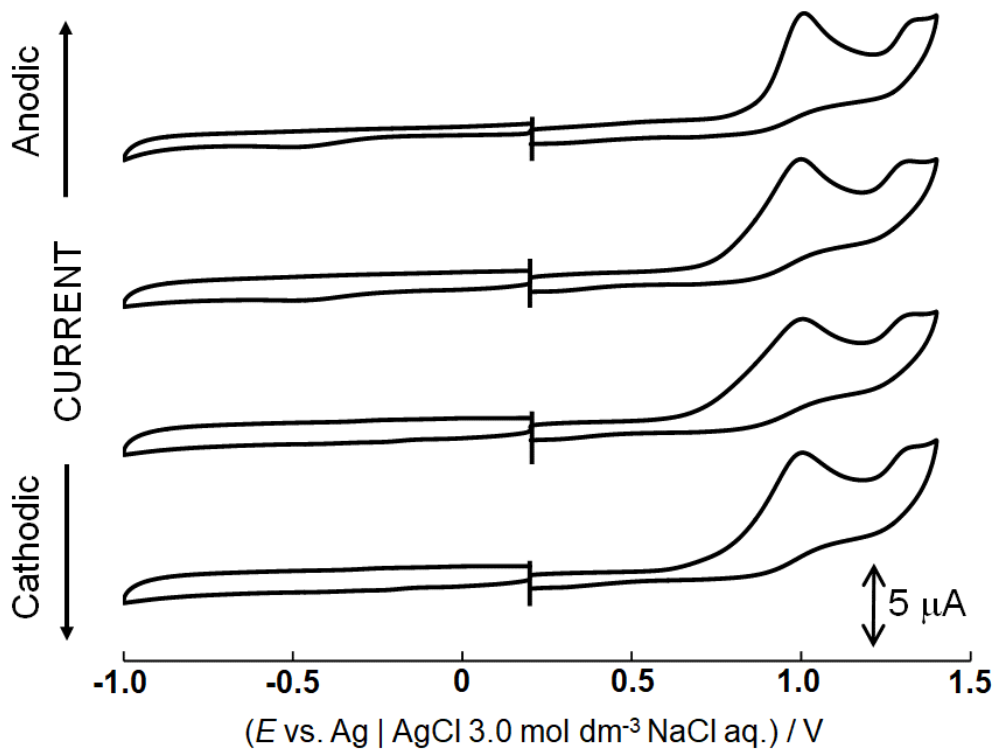

Fig. S7 Cyclic voltammograms of *cis*-[$Ru^{II}(NH_2C_6H_5)_2(bpy)_2$]($CF_3SO_3$)$_2$ [**1**](CF_3SO_3)$_2$ in water-dimethyl sulfoxide (2:3 (*v*/*v*)) at pH 2.77, 4.65, 6.06 and 7.90.

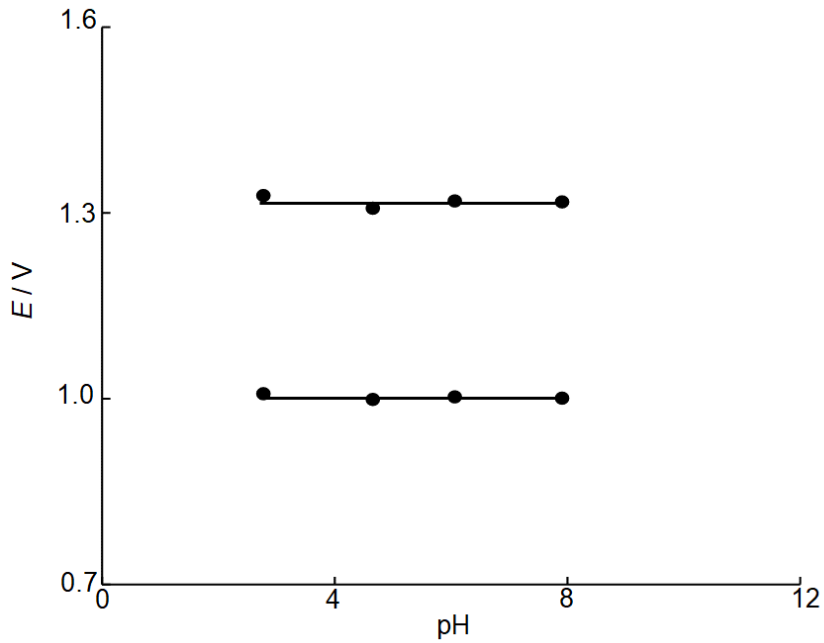

Fig. S8 Pourbaix diagrams of *cis*-[$Ru^{II}(NH_2C_6H_5)_2(bpy)_2$]($CF_3SO_3$)$_2$ [**1**](CF_3SO_3)$_2$.

DFT Calculations

All calculations were performed with the Gaussian 09 program. The geometry optimizations were performed at the B3LYP level of density functional theory with the Los Alamos effective core potential plus DZ (LANL2DZ).

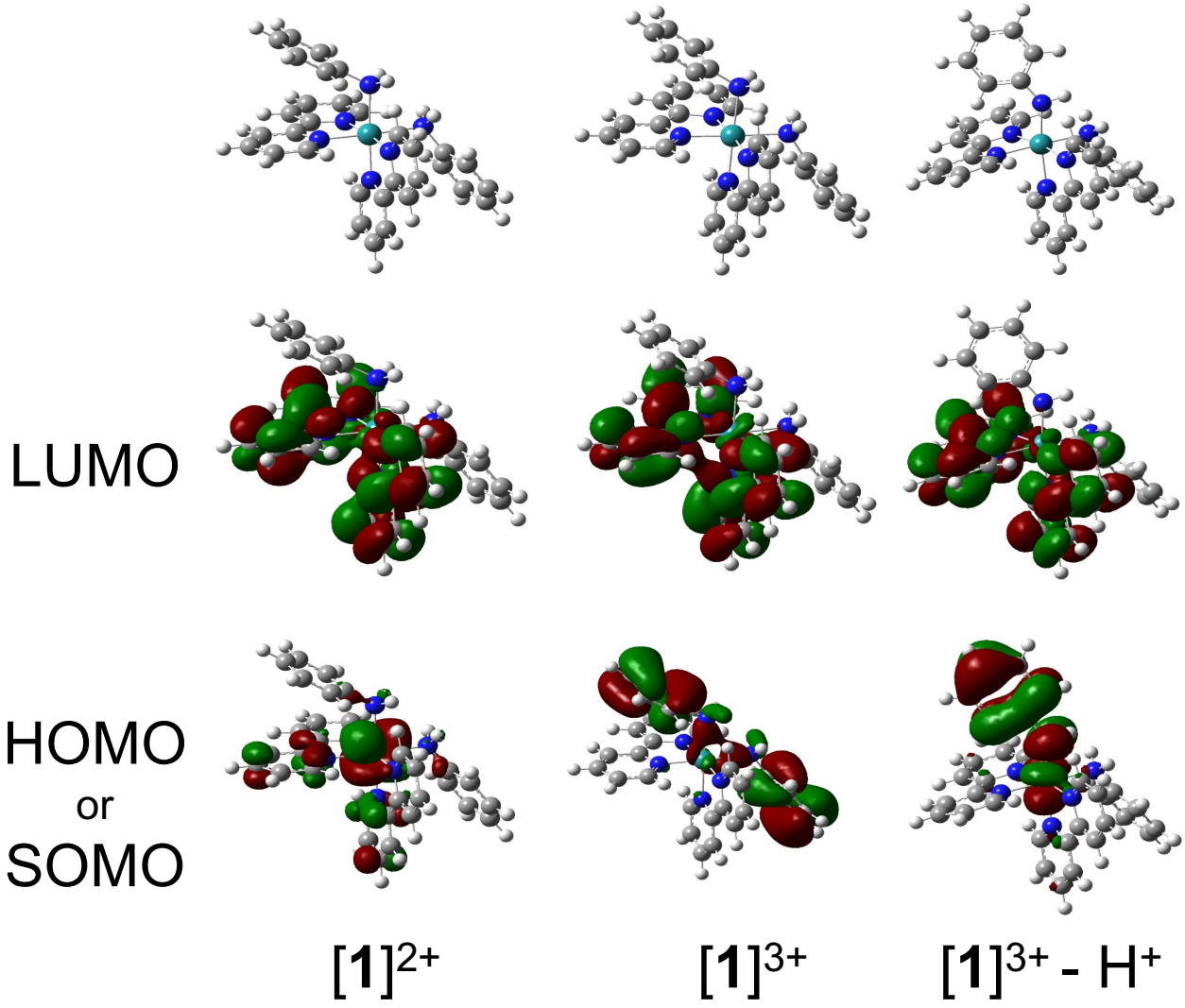

Fig. S9 LUMO and HOMO or SOMO of $[Ru^{II}(NH_2C_6H_5)_2(bpy)_2]^{2+}$ ([**1**]$^{2+}$), $[Ru(NH_2C_6H_5)_2(bpy)_2]^{3+}$ ([**1**]$^{3+}$), $[Ru(NHC_6H_5)(NH_2C_6H_5)(bpy)_2]^{2+}$ ([**1**]$^{3+}$ - H^+).

Table S2 Metric parameters of $[Ru^{II}(NH_2C_6H_5)_2(bpy)_2]^{2+}$ $[\mathbf{1}]^{2+}$, the one-electron oxidized complex $[\mathbf{1}]^{3+}$, and the deprotonated species of the one-electron oxidized complex $[\mathbf{1}]^{3+}$-H^+.

	$[\mathbf{1}]^{2+}$	$[\mathbf{1}]^{3+}$	$[\mathbf{1}]^{3+}$-H^+
Ru-N1$_{aniline}$	2.2592	2.2305	2.2478
Ru-N2$_{aniline\ or\ aminyl}$	2.2592	2.2305	2.0366
Ru-N3-N6$_{bpy}$	2.0767 - 2.1102	2.0821 - 2.1207	2.0826 - 2.1234
N1–C1	1.4767	1.4900	1.4747
N2–C7	1.4767	1.4900	1.3905
C1-C2	1.4065	1.4069	1.4064
C2-C3	1.4066	1.4069	1.4070
C3-C4	1.4090	1.4100	1.4086
C4-C5	1.4076	1.4087	1.4079
C5-C6	1.4079	1.4081	1.4073
C6-C1	1.4059	1.4059	1.4063
C7-C8	1.4065	1.4069	1.4352
C8-C9	1.4066	1.4069	1.3968
C9-C10	1.4090	1.4100	1.4143
C10-C11	1.4076	1.4087	1.4139
C11-C12	1.4079	1.4081	1.3984
C12-C7	1.4059	1.4059	1.4281

Table S3 Molecular orbital of $[Ru^{II}(NH_2C_6H_5)_2(bpy)_2]^{2+}$ $[\mathbf{1}]^{2+}$ and $[Ru^{II}(\mathit{N}HC_6H_4\mathit{N}C_6H_5)(bpy)_2]^{2+}$ $[\mathbf{4}]^{2+}$

complex	MO	eV of energy	% of composition	
			Ru	Ligand*
$[Ru^{II}(NH_2C_6H_5)_2(bpy)_2]^{2+}$ ($[\mathbf{1}]^{2+}$)	LUMO	-7.74	3	66
	HOMO	-11.07	64	6
$[Ru^{II}(\mathit{N}HC_6H_4\mathit{N}C_6H_5)(bpy)_2]^{2+}$ ($[\mathbf{4}]^{2+}$)	LUMO	-8.73	16	69
	HOMO	-11.10	38	39

*Ligand: aniline or diimine ligand

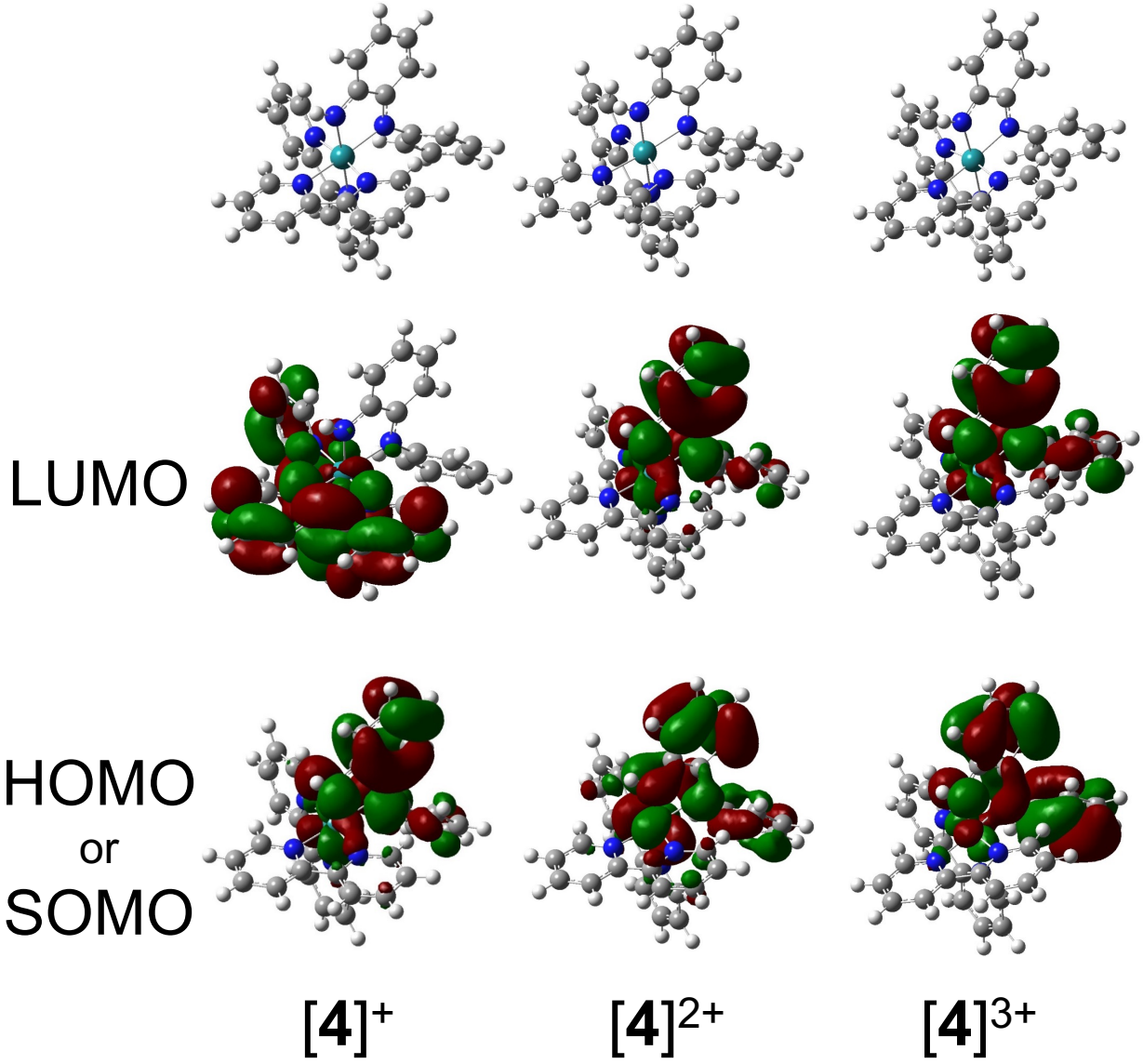

Fig. S10 LUMO and HOMO or SOMO of $[Ru^{II}(NHC_6H_4NC_6H_5)(bpy)_2]^{2+}$ $[\mathbf{4}]^{2+}$, $[Ru(NHC_6H_4NC_6H_5)(bpy)_2]^{+}$ $[\mathbf{4}]^{+}$ (one-electron reduced form) and $[Ru(NHC_6H_4NC_6H_5)(bpy)_2]^{3+}$ $[\mathbf{4}]^{3+}$ (one-electron oxidized form) .

Oxidation of anilne complexes.

Oxidation reaction of *cis*-[Ru($NH_2C_6H_4$(4-CH_3))$_2$(bpy)$_2$](CF_3SO_3)$_2$ [**2**](CF_3SO_3)$_2$ in H_2O by four molar equivalents of oxidants ($(NH_4)_4[Ce^{IV}(SO_4)_4]\cdot 2H_2O$) were carried out (Fig. S11). The spectrum after 2 hours was consistent with that of *cis*-[Ru(*N*HC_6H_3(4-CH_3)*N*C_6H_4(4-CH_3))(bpy)$_2$](PF_6)$_2$ [**5**](PF_6)$_2$. The formation of [**5**]$^{2+}$ occurs more slowly than that of [**4**]$^{2+}$. Assuming these oxidation reactions are pseudo-first-order reactions, the rate constants in the oxidation reaction of [**1**]$^{2+}$ and [**2**]$^{2+}$ were roughly estimated to 7×10^{-4} and 3×10^{-4}, respectively.

An oxidation reaction of *cis*-[Ru($NH_2C_6H_5$)$_2$(bpy)$_2$](CF_3SO_3)$_2$ [**1**](CF_3SO_3)$_2$ by four molar equivalents of oxidants in the presence of ten molar equivalents of radical scavengers (2,2,6,6-tetramethylpiperidine 1-oxyl) was carried out (Fig. S12). Changes in absorbances were observed during the oxidation reactions of *cis*-[Ru^{II}($NH_2C_6H_5$)$_2$(bpy)$_2$](CF_3SO_3)$_2$ [**1**](CF_3SO_3)$_2$ (520 nm, black) and *cis*-[Ru($NH_2C_6H_4$(4-CH_3))$_2$(bpy)$_2$](CF_3SO_3)$_2$ [**2**](CF_3SO_3)$_2$ (524 nm, blue) as shown in Fig. S13.

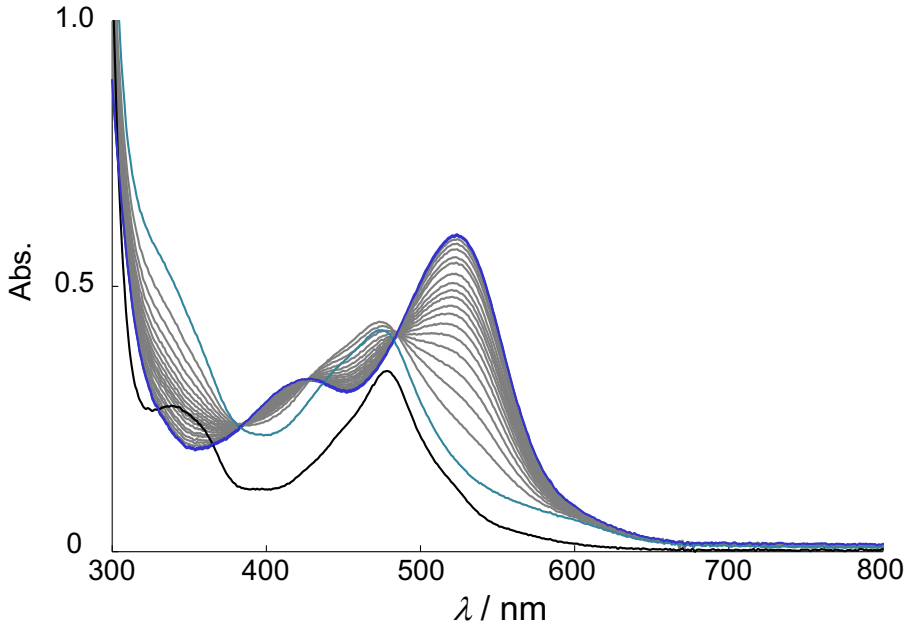

Fig. S11 Oxidation reaction of *cis*-[Ru($NH_2C_6H_4$(4-CH_3))$_2$(bpy)$_2$](CF_3SO_3)$_2$ [**2**](CF_3SO_3)$_2$ in the presence of four molar equivalents of the oxidant; before oxidation (black), after oxidation 30 seconds (green), and 2 hours (blue).

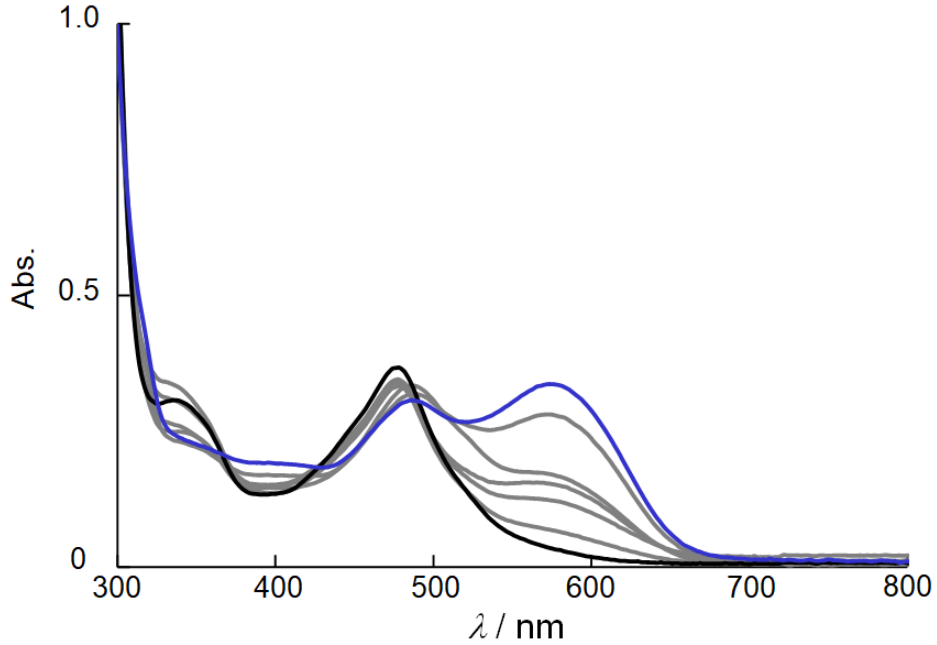

Fig. S12 Oxidation reaction of *cis*-$[Ru(NH_2C_6H_5)_2(bpy)_2](CF_3SO_3)_2$ [**1**]$(CF_3SO_3)_2$in the presence of four molar equivalents of the oxidant and 10 equivalents of radical scavengers before oxidation (black) and after oxidation (blue).

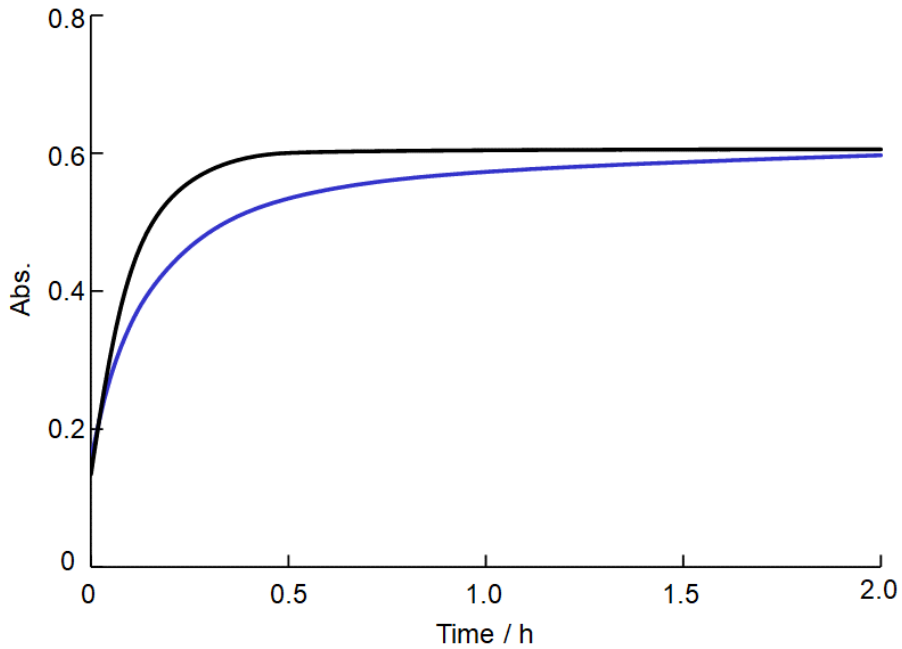

Fig. S13 Change in absorbance during the oxidation reactions of *cis*-$[Ru^{II}(NH_2C_6H_5)_2(bpy)_2](CF_3SO_3)_2$ [**1**]$(CF_3SO_3)_2$ (black) and *cis*-$[Ru(NH_2C_6H_4(4\text{-}CH_3))_2(bpy)_2]$-$(CF_3SO_3)_2$ [**2**]$(CF_3SO_3)_2$ (blue).

X-ray structural analysis

The crystallographic data and selected bond distances and angles are summarized in Table S4. Structures of *cis*-$[Ru(NH_2C_6H_4(4\text{-}CH_3))_2(bpy)_2]^{2+}$ ($[\mathbf{2}]^{2+}$) and *cis*-$[Ru(NHC_6H_3(4\text{-}CH_3)NC_6H_4(4\text{-}CH_3))(bpy)_2]^{2+}$ ($[\mathbf{5}]^{2+}$) are shown in Fig. S14 and S15.

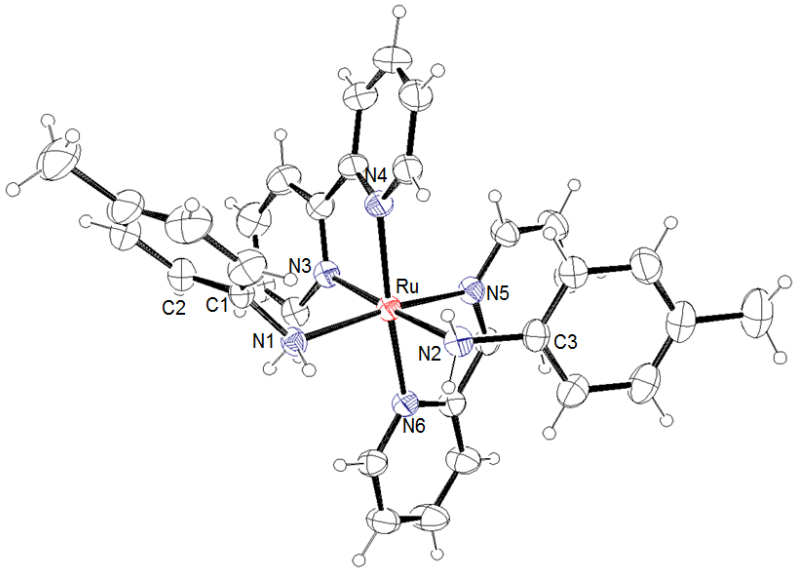

Fig. S14 Structure of *cis*-$[Ru(NH_2C_6H_4(4\text{-}CH_3))_2(bpy)_2]^{2+}$ $[\mathbf{2}]^{2+}$ showing 50 % thermal ellipsoid probability.

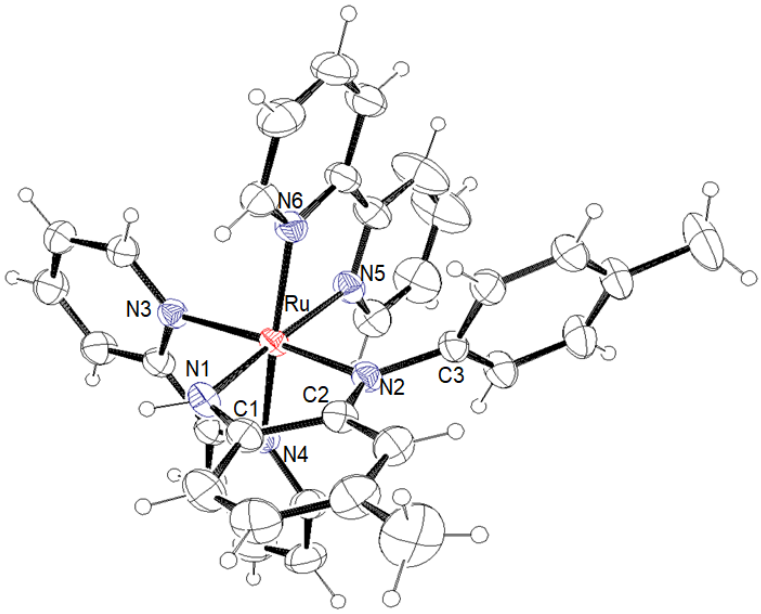

Fig. S15 Structure of *cis*-$[Ru^{II}(NHC_6H_3(4\text{-}CH_3)NC_6H_4(4\text{-}CH_3))(bpy)_2]^{2+}$ $[\mathbf{5}]^{2+}$ showing 50 % thermal ellipsoid probability.

Table S4 Crystallographic data of dianiline and diimine complexes

	[**1**]$^{2+}$	[**2**]$^{2+}$	[**3**]$^{2+}$	[**4**]$^{2+}$	[**5**]$^{2+}$
formula	$C_{34}H_{30}N_6F_6O_6RuS_2$	$C_{36}H_{34}N_6F_6O_6RuS_2$	$C_{34}H_{26}F_{10}N_6O_6RuS_2$	$C_{32}H_{26}N_6P_2F_{12}Ru$	$C_{34}H_{30}F_{12}N_6P_2Ru$
molecular weight	897.83	925.88	969.80	885.60	913.65
crystal color	red	red	red	black	black
habit	block	block	block	block	block
crystal dimensions	0.10 x 0.10 x 0.10	0.10 x 0.10 x 0.10	0.10 x 0.10 x 0.13	0.13 x 0.13 x 0.16	0.10 x 0.10 x 0.10
crystal system	monoclinic	monoclinic	triclinic	monoclinic	triclinic
space group	$P2_1/n$ (#14)	$P2_1/n$ (#14)	P-1 (#2)	$P2_1/n$ (#14)	P-1 (#2)
a / Å	11.25790(10)	11.23880(10)	10.00630(10)	13.31180(10)	13.27250(10)
b / Å	17.1076(2)	22.2125(3)	10.2443(2)	18.79730(10)	13.51310(10)
c / Å	19.0176(2)	15.9788(2)	10.4305(2)	13.97790(10)	13.79670(10)
β / °	95.9820(10)	91.1880(10)	93.0320(10)	97.4170(10)	103.0590(10)
V / Å^3	3642.76(7)	3988.12(8)	946.35(3)	3468.37(4)	1977.56(3)
Z	4	4	1	4	2
D_c / g cm^{-3}	1.637	1.542	1.702	1.696	1.534
μ / cm^{-1} (Cu$K\alpha$)	5.311	4.869	5.321	5.440	4.789
T /K	298.15	298.15	298.15	298.15	298.15
transmission factors	0.85671 – 1.00000	0.80411 – 1.00000	0.32571 – 1.00000	0.93290 – 1.00000	0.53776 – 1.00000
$2\theta_{max}$ / °	55.0	55.0	55.0	55.0	55.0
total reflections	25740	29966	9898	25055	23385
unique reflections	7325	8005	3755	6959	7921
R_1 [a)] ($I > 2.00\sigma(I)$)	0.0324	0.0520	0.0543	0.0346	0.0500
wR_2 [b)] ($I > 10.00\sigma(I)$)	0.0839	0.1548	0.1540	0.0970	0.1417
R_{int}	0.0296	0.0311	0.0829	0.0266	0.0355
GOF	1.068	1.157	1.076	1.064	1.050

a) $R = \Sigma \, ||F_o| - |F_c|| \, / \, \Sigma \, |F_o| \; (I > 2\sigma(I))$, b) $wR_2 = [\Sigma(w(F_o^2 - F_c^2)^2) \, / \, \Sigma \, w(F_o^2)^2]^{1/2}$